

Implications of tristability on localization phenomena: a necking bifurcation's tale

Edem Kossi Akakpo¹, Marc Haelterman¹, Francois Leo¹, and Pedro Parra-Rivas^{2,1*}

¹ OPERA-photonics, Université libre de Bruxelles,
50 Avenue F. D. Roosevelt,
CP 194/5, B-1050 Bruxelles, Belgium

² Dipartimento di Ingegneria dell'Informazione,
Elettronica e Telecomunicazioni,
Sapienza Università di Roma,
via Eudossiana 18, 00184 Rome, Italy

We analyze the implication of tristability on localization phenomena in one-dimensional extended dissipative systems. In this context, localized states appear due to the interaction and locking of front waves connecting different extended states. In the tristable regime investigated here two extended uniform states coexist with one periodic Turing pattern. This scenario leads to the transition from the standard-homoclinic-snaking-related localized states associated with uniform-pattern bistability to the collapsed-homoclinic-snaking-related states which arise in a uniform-bistable configuration. We find that this transition is mediated by the emergence of hybrid states through codimension-two necking bifurcations. To perform this study we use bifurcation analysis on a non-variational mean-field model describing the spatiotemporal dynamics of light pulses in passive Kerr cavities.

I. INTRODUCTION

The formation of localized states, hereafter LSs, in one-dimensional extended systems which are far from thermodynamic equilibrium is closely related to the concept of front wave interaction and locking [1–4]. Front waves, also known as domain walls or switching waves, consist in smooth interphases connecting different extended, and coexisting, states such that the nature and morphology of the former are determined by the latter. We can mainly classify fronts in two groups: those connecting two uniform, or homogeneous, states, that we will call *uniform fronts*, and those appearing as interphases between uniform and non-uniform, or patterned, states, which we refer to as *patterned front*.

Independently of the group, two fronts with different polarities (e.g., imagine a kink and anti-kink in the uniform scenario) may lock to one another leading to the formation of LSs with different extensions (i.e., widths) and shapes. However, the nature of the fronts involved in such interaction determines the locking mechanism, and therefore the bifurcation structure, which in this context is known as *homoclinic snaking* [5, 6].

In a uniform bistable configuration, i.e., when the coexisting states are uniform, the LSs that emerge correspond to an isolated plateau of one uniform state embedded in the other one, and undergo the so-called *collapsed homoclinic snaking* [6, 7]. When the interaction involves patterned fronts, the LSs formation, much more complex in this case, is related to a different organization known as *standard homoclinic snaking* [5, 8].

These bifurcation structures are quite well understood in a bistable configuration, i.e., when only two extended states coexist within the same parameter range, and have been widely studied in far apart scientific disciplines such

as nonlinear optics [8–12], reaction-diffusion systems [13–15], or neuroscience [16], to only cite a few.

Things can be quite different when more than two extended states coexist. In this case, more complex hybrid fronts may appear, leading to important implications regarding the formation of new and exotic LSs. The implications of uniform-pattern-uniform tristability on the formation and bifurcation structure of LSs was tackled in a pant ecology context using Klausmeier-Gray-Scott model [14]. However, although a transition between the previous snaking organizations was found, the main mechanism, in bifurcation terms, behind such metamorphosis was veiled. This mechanism has been recently identified in the prototypical, and variational, Swift-Hohenberg equation, and relies on the occurrence of a cascade of codimension-two (codim-2) *necking bifurcations* [17]. In these codim-2 points, two fold bifurcations collide and separate afterward, yielding the reorganization of the LSs bifurcation structures. Despite this discovery, the generality of these results, and therefore their extension, to other scenarios, particularly non-variational ones, was not demonstrated.

In this regard, the main scope of this work is to prove such generality. To do so, we use a modified version of the Lugiato-Lefever equation (LLE), a non-variational model (i.e., with nongradient-like dynamics [18]) describing the evolution of the complex amplitude of the electric field inside a passive Kerr optical cavity [19, 20]. Besides the importance of understanding this transition from a fundamental point of view, this knowledge will have important implications from a more practical perspective since it could provide new ways for optical cavity soliton and frequency comb generation [21, 22].

The paper is organized as follows. In Section II we introduce a modified version of the LLE equation describing Kerr passive cavities in the presence of fourth-order dispersion (FOD). This dispersion effect is essential for the emergence of tristability. Later, in Section III we

* Corresponding author: pedro.parra-rivas@uniroma1.it

introduce the necessary background for understanding stability properties of the uniform and extended states and present the tristable scenario. Section IV unveils the LSs bifurcation structure transition taking place in the system. The necking bifurcation organizing these transitions is presented in Section V. Finally, in Section VI we provide a short discussion and the main conclusions of our work.

II. MODEL AND METHODS

In the mean-field approximation, passive Kerr dispersive cavities can be described by the LLE [20, 23]. Considering chromatic dispersion up to fourth-order, and neglecting the contribution of third-order dispersion (TOD), the normalized LLE reads

$$\partial_t A = -(1 + i\Delta)A - id_2 \partial_x^2 A + id_4 \partial_x^4 A + i|A|^2 A + S, \quad (1)$$

where A is the complex field amplitude, t represents the time coordinate, and x the space in spatial cavities, the fast time in fiber cavities or angular variable in microresonators. The losses are normalized to 1, Δ is the phase detuning from the closest cavity resonance and S in the driving field amplitude. With this normalization, $d_2 = \text{sign}(\beta_2) = \pm 1$ and $d_4 \equiv \beta_4 \alpha / (6L|\beta_2|^2)$, where α represents the losses, L is the cavity length, and β_2 and β_4 represent the second-order dispersion (SOD) and FOD coefficients, respectively.

In this work we are interested in studying LSs which are symmetric through the transformation $x \rightarrow -x$. This is the reason why we have neglected TOD effects. Besides, as we will see in the next section, the presence of FOD is necessary for the emergence of uniform-pattern-uniform tristability, which is otherwise absent [12]. To attain such tristable configuration we fix $d_2 = -1$ and $d_4 = 1$. This regime was investigated in 2010 when the positive effect of FOD for stabilizing standard-homoclinic-snaking-related dark LSs was identified [24]. We have recently used Eq. (1) for studying the formation of collapsed-snaking-related LSs, but using a rather different dispersion configuration (i.e., $d_2 = 1$ and $d_4 > 0$) [25]. Moreover, this model has been also exploited for unveil the formation of bright and dark LSs in pure quartic dispersive cavities [26].

To perform this bifurcation analysis, we mainly apply path-continuation algorithms based on a predictor-corrector method [27, 28] using the free software package AUTO-07p [29]. With this procedure, we are able to compute not only the stable but also the unstable state solutions, unveiling their connection. The spectral stability of these states is then determined by solving the linear eigenvalue problem

$$\mathcal{L}\psi = \sigma\psi, \quad (2)$$

where \mathcal{L} is the linear operator associated with the right hand side of Eq. (1) evaluated a given steady state, and ψ is the eigenmode corresponding to the eigenvalue σ .

The time-independent state is stable if $\text{Re}[\sigma] < 0$, and unstable otherwise. If by varying a control parameter of the system, let's say p , this transition occurs at the value $p = p_c$ (i.e., $\text{Re}[\sigma(p_c)] = 0$), we say that a local bifurcation takes place at p_c [30, 31].

For representing the different type of states and their bifurcation structure, we compute bifurcation and phase diagrams where we show the modification of a given bifurcation measure as a function of the main parameter of the system. Here, we choose as measure the solutions energy (i.e., the L_2 -norm)

$$E^2 \equiv L^{-1} \int_{-L/2}^{L/2} |A(x)|^2 dx,$$

and S and Δ as main control parameters of the system.

III. TRISTABILITY AND EXTENDED STEADY STATES

When working with dissipative extended systems, one essential task is to identify the different types of extended time-independent states and their stability. In this regard, the simplest time-independent solution is the uniform or homogeneous steady state (HSS) solution A_h , which satisfies the algebraic equation [19, 20]

$$S^2 = I_h^3 - 2\Delta I_h^2 + (1 + \Delta^2)I_h, \quad (3)$$

for $I_h \equiv |A_h|^2$. For a fixed value of Δ , this expression defines a nonlinear dependence between the intracavity intensity I_h and the pump S which can be seen in Fig. 1(a) for $\Delta = 2.5$. In this regime, the system shows uniform multistability, i.e., for the same value of S three HSSs, namely A_h^b , A_h^m , and A_h^t , coexist. These states are connected at two folds, or turning points, located at the positions

$$I_h^{l,r} \equiv \frac{1}{3} \left(2\Delta \pm \sqrt{\Delta^2 - 3} \right). \quad (4)$$

As a function of Δ , these folds define two curves in the (Δ, S) -parameter diagram shown in Fig. 1(c) [see solid black lines]. Here, the vertical pointed line corresponds to the diagram plotted in Fig. 1(a). Decreasing Δ , eventually, these folds annihilate one another in a codim-2 cusp bifurcation, marked with C_h , which occurs at $\Delta = \sqrt{3}$. Similarly, one can look at this scenario by fixing S and varying Δ . As result, one obtains the nonlinear resonance of the cavity which is solution of the equation $\Delta = I_h \pm \sqrt{(S/I_h)^2 - 1}$. This resonance is plotted in Fig. 1(b) for $S = 1.65$.

To establish the stability of these uniform states we perform a linear stability analysis by studying how A_h reacts against non-uniform perturbations of the form $\propto e^{\sigma t + ikx}$. This leads to the linear eigenvalue problem (2). For $k = 0$, A_h undergoes a pair of saddle-node bifurcations $\text{SN}_h^{l,r}$ whose positions are given by the folds Eq. (4). For non-uniform perturbations ($k \neq 0$), A_h encounters a pair of Turing instabilities which are marked

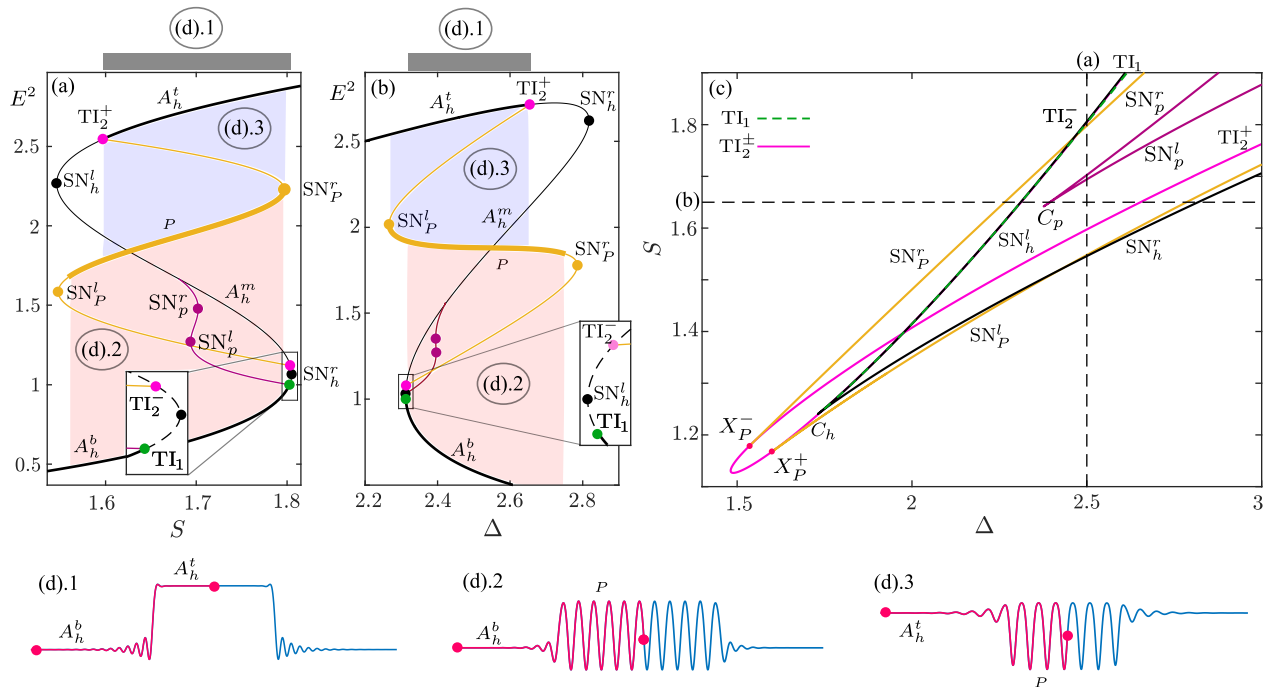


FIG. 1. **Uniform-pattern-uniform tristable regime.** Panel (a) shows the modification of the uniform state A_h (see black curve) and the Turing pattern P (see yellow curve) energy E^2 as a function of S for $\Delta = 2.5$. The gray bar on the top defines the region of uniform bistability. The blue and red shaded colored areas correspond to uniform-pattern bistability. Panel (b) shows the nonlinear cavity resonance for $S = 1.65$. In both cases we mark the saddle-node bifurcations of the pattern $SN_P^{l,r}$, those of the uniform state $SN_h^{l,r}$, and the Turing bifurcations TI_1 and TI_2^\pm . Stable (unstable) are illustrated using solid thick (thin) lines. Panel (c) shows the modifications of $SN_h^{l,r}$, $SN_P^{l,r}$, TI_1 and TI_2^\pm in the (Δ, S) -parameter space. The vertical dashed line corresponds to the situation shown in (a); the horizontal one to the nonlinear cavity resonance shown in (b). We also mark the codim-2 points C_h and X_P^\pm . In (d) we show some examples of the type of LSs (blue) and front waves (pink) that can form in the bistable scenarios shown in (a) and (b).

TI_1 and TI_2 in Fig. 1. These instabilities appear at different positions and have different critical wave-numbers. TI_1 [see green dot in the close-up view of Figs. 1(a),(b)] occurs, for $\Delta > 7/4$, at $I_h = I_1^c \equiv 1$ with wave-number

$$k_1^c = \sqrt{\frac{1 + \sqrt{1 + 4(\Delta - 2)}}{2}}. \quad (5)$$

The wave-number and position associated with TI_2 (pink) read $k_2^c = 1/\sqrt{2}$ and

$$I_2^c = \frac{4\Delta + 1}{6} \pm \frac{\sqrt{(\Delta + 1/4)^2 - 3}}{3},$$

with $\Delta > \sqrt{3} - 1/4$. The parts of the A_h -solution curves which are Turing unstable are depicted using thin solid lines, while for those which are stable we use solid thick lines. The modification of these bifurcations with varying Δ are shown in Fig. 1(c) using a pink line for TI_2 and a green dashed line for TI_1 . At this point we can clearly establish the uniform-bistability region where $A_h^{b,t}$ coexist and are both stable. This regions is depicted using a gray shaded box on top of Figs. 1(a),(b). From TI_2 , a spatially periodic Turing pattern P emerges with a wave-number which is approximately equal to k_2^c . For the parameter values we choose here, this pattern arises subcritically

from I_2^\pm [see yellow curve Fig. 1(a)] and stabilizes at the SN bifurcations $SN_P^{l,r}$. The modification of these folds in the (Δ, S) -parameter space is depicted in Fig. 1(c). With decreasing Δ , this Turing pattern becomes supercritical at the codim-2 points X_P^\pm , which correspond to degenerate Turing instabilities, from where the supercritical and subcritical configurations arise.

Regarding TI_1 , another unstable subcritical Turing pattern arise from I_1^c , now with a typical wavelength $2\pi/k_1^c$ [see magenta curve in Figs. 1(a),(b)]. This state undergoes a pair of fold bifurcations $SN_P^{l,r}$ that leave their stability unchanged, i.e., this pattern never become stable. With increasing Δ , $SN_P^{l,r}$ separate from one another. Decreasing Δ , however, they come closer and eventually they annihilate each other in the cusp bifurcation C_p [see magenta lines in Figs. 1(c)]. This pattern always arise subcritically from A_h^b .

The stable branch of the P -pattern [see tick solid line in Figs. 1(a),(b)] and stable sections of A_h determine a pair of pattern-uniform bistability regions colored using shaded blue and red [see Figs. 1(a),(b)]. These regions, together with the uniform-bistability interval marked with the gray bar, form a tristable uniform-pattern-uniform scenario. In this context [see Fig. 1(d)], different front states (see pink profile) and LSs (see blue

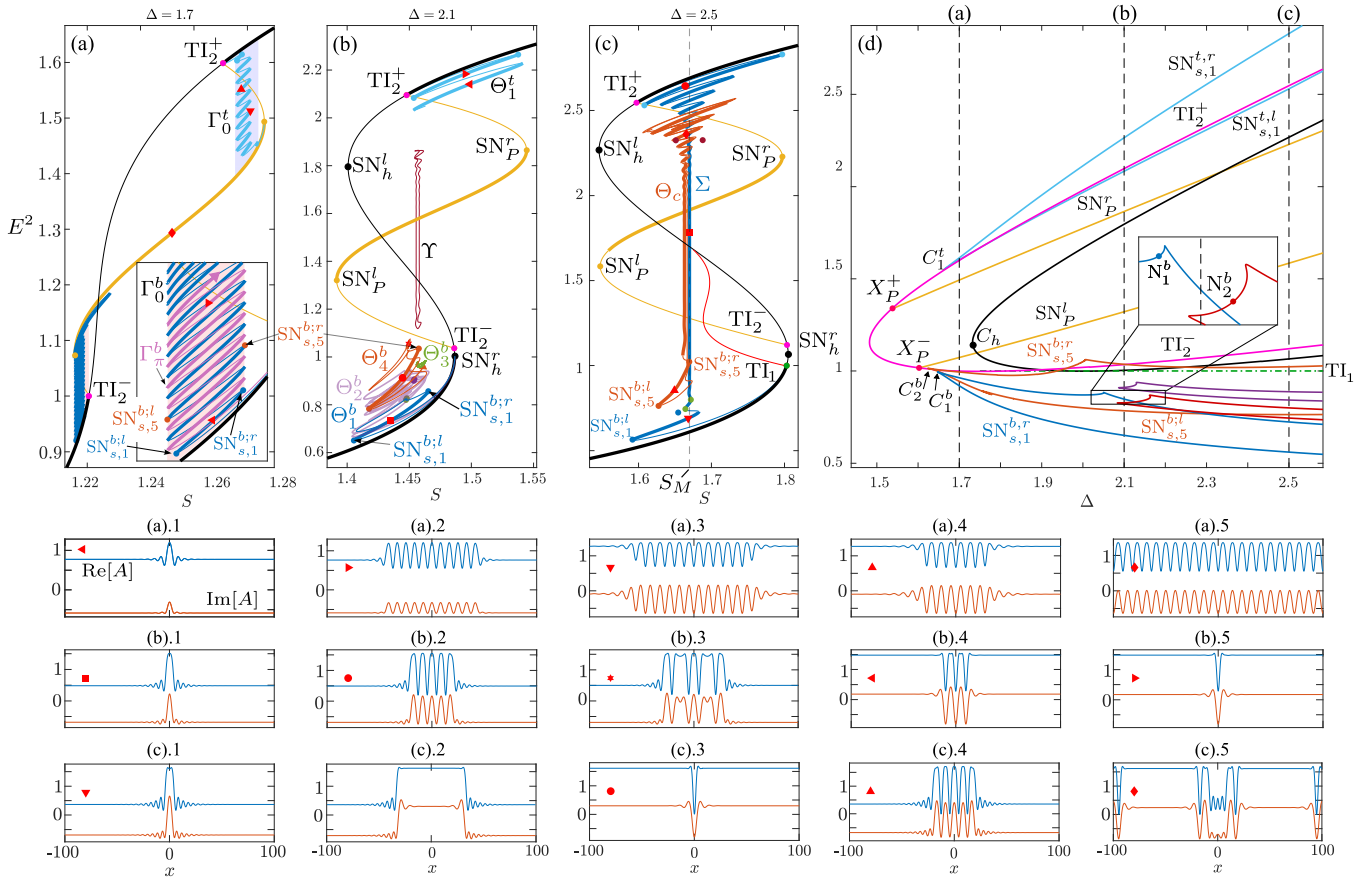


FIG. 2. **Transition between the standard and collapsed homoclinic snaking in a uniform-pattern-uniform tristable regime.** Panel (a) shows the standard homoclinic regime for $\Delta = 1.7$. The bifurcation diagrams $\Gamma_{0,\pi}^b$ and Γ^t correspond to bright and dark LSs, respectively. The yellow curve represents the Turing pattern and the red- and blue-shaded boxes represent the uniform-pattern bistability regions. Panels (a).1-5 illustrate examples of LSs along these diagrams. Panel (b) corresponds to the transition region and shows the emerging isolas $\Theta_{1,2,3,4}^b$, Θ_1^t and Υ . LSs on these curves are plotted in panels (b).1-5. Panel (c) represents the collapse snaking region (see Σ diagram), where other complex isolas also exist (see Θ_c). Examples of states belonging to these branches are depicted Figs. 2(c).1-5. Panel (d) shows the modification of the main bifurcation lines as a function of E^2 and Δ .

profile) may form. The existence of these states in the different parameter regions of the systems are marked in Figs. 1(a),(b). In 1D extended systems, the interaction and locking of these fronts is well understood and we refer to the following works for more details [4, 5, 8, 12, 32].

The coexistence between all these bistable configurations changes with Δ : decreasing Δ , uniform bistability disappears at C_h and only the upper and bottom uniform-pattern bistable regimes persist until reaching X_P^\pm ; above C_h uniform-pattern-uniform tristability emerges, increasing its extension with Δ .

IV. BIFURCATION STRUCTURE TRANSITION IN TRISTABLE REGIMES

Once the uniform and pattern states have been investigated, and their overlapping regions and variety of fronts identified, it is now time for studying the emergence of LSs.

To do so, we perform a detailed and systematic bi-

furcation analysis based on path-parameter continuation techniques and spectral analysis, as already introduced in Section II. The main results are depicted in Fig. 2 where the modification of the time-independent extended and localized states bifurcation structure is shown in terms of their energy E^2 for different values Δ .

Figure 2(a) depicts, for $\Delta = 1.7$, the LSs bifurcation structure which arises through the locking of patterned fronts like those shown in Figs. 1(d).2 and 1(d).3 in a pure uniform-pattern bistable regime. Here, the periodic pattern P emerge subcritically from the Turing bifurcations TI_2^\pm (see position I_2^\pm located at the bottom and top of the HSS diagram), creating two bistable regimes which are colored in shaded blue and red. Note that, for this value of Δ , there is not uniform bistability and the uniform-pattern bistable regimes do not overlap.

Within these bistable regimes, the locking of patterned-fronts yields the creation of dark and bright LSs which organize in terms of *standard homoclinic snaking* [5]. In this bifurcation structure the solution curves oscillates back-and-forth within the so called pin-

ning region [5, 8, 33]. Along this diagram, LSs consist in a slug of the periodic pattern [see Fig. 2(a).5] embedded within a uniform background. Some examples of these states are illustrated in Figs. 2(a).1-4.

These LSs emerge from TI_2^\pm subcritically in pairs yielding two families of snaking curves that we call $\Gamma_{0,\pi}$ [12, 33]. While Γ_0 corresponds to LSs with a odd number of pattern wave-lengths (i.e., peaks), in Γ_π the number of peaks are even. These two families are shown for the bright LSs case [see $\Gamma_{0,\pi}^b$ in Fig. 2(a)]. Regarding dark LSs we only plot Γ_0^t for simplicity. Along these diagrams there is an alternation between stable and unstable states, which are separated by SN bifurcations that we label $\text{SN}_{s,i}^{l,r}$, with i representing the numbers of pattern peaks within the LS solution branch. These left/right bifurcations limit two well defined LS-multistability regions whose width is conserved as varying E^2 [see close-up view in Fig. 2(a) as reference]. While the snaking associated with the bright states exists in the absence of d_4 [8, 12], the dark ones are stabilized precisely due to the presence of this dispersive effect [24].

The modification of the main bifurcations of the system with Δ , and therefore the modification of the LSs bifurcation structure, is reflected in the (E^2, Δ) -phase diagram shown in Fig. 2(d). The bifurcation diagram illustrated in Fig. 2(a) corresponds to a slice of the phase diagram for $\Delta = 1.7$ [see first vertical dashed line].

This diagram shows in yellow $\text{SN}_P^{l,r}$, in black $\text{SN}_h^{l,r}$ and in pink TI_2^\pm . The codim-2 point where the Turing patterns become subcritical are marked with the X_P^\pm as in Fig. 1(c). The bifurcations $\text{SN}_P^{l,r}$ emanate from this point. The cusp codim-2 point shown in Fig. 1(c) here corresponds to the fold marked with C_h . Besides, $\text{SN}_{s,i}^{b;l,r}$ for $i = 1, 5$ and $\text{SN}_{s,1}^{t;l,r}$ are plotted. Here, the super-index b (or t) refers to the bottom (top) part of the diagram shown in Fig. 2(a). Decreasing Δ these bifurcation pairs annihilate one-another in different cusp points $C_i^{b,t}$, and with them their associated LSs.

Just a bit after the emergence of the uniform-bistability (i.e., for $\Delta > \sqrt{3}$) the standard homoclinic snaking scenario breaks down, leading to the configuration depicted in Fig. 2(b) [$\Delta = 2.1$] where a sequence of isolas (i.e., disconnected closed bifurcation curves) is formed. The blue isola in the bottom, Θ_1^b , corresponds to the single-peak LS depicted in Fig. 2(b).1 and still arises from TI_2^- . The stable branch in this curve is the deformation of the first stable branch of Γ_0^b [see Fig. 2(a)]. Similarly occurs for all LSs, leading to an intricate entangle of isolas. Here, for simplicity, we also show the isolas $\Theta_{2,3}^b$ and Θ_4^b . The latter is related to the five-peak state plotted in Fig. 2(b).2 and to the *hybrid* LSs formed through a combination of the two locking mechanism described previously [see Fig. 2(b).3].

In a similar fashion, the homoclinic snaking Γ_0^t gets disconnected forming another sequence of isolas. One of these isolas, Θ_1^t , is depicted in Fig. 2(b). The stable branches of Θ_1^t correspond to the dark LSs shown in Fig. 2(b).4 and 2(b).5.

In-between isolas $\Theta_{1,2,3,4}^b$ and Θ_1^t , approximately in the middle of the uniform-pattern bistability region, a new type of isola (Υ) appears. All along this isola, LSs form through the locking of uniform-fronts. Υ is the main embryonic structure underlying the collapsed snaking formation.

By increasing Δ , $\Theta_{1,2,3}^b$ and Υ will merge leading to the recombination of the LSs branches forming Υ' [see Fig. 4(b)], which eventually, will yield the appearance of the collapse homoclinic snaking Σ shown in Fig. 2(c) for $\Delta = 2.5$ [see vertical dashed line in Fig. 2(d)]. The emergence of this bifurcation structure is associated with the locking of uniform fronts [see Fig. 1(d).1] and leads to a broad variety of dark and bright LSs [see Fig. 2(c).1-3]. This bifurcation structure oscillates back and forth around the uniform Maxwell point (S_M) of the system in a damped fashion which is intrinsically related to the LSs formation in this regime [12, 34]. Here, in contrast to the standard case, LSs multistability decreases when moving away from S_M . The collapsed snaking exist in other operational regimes involving d_4 [25], and also in the absence of fourth order dispersion [12]. However, as far as we known, collapsed snaking has not been previously predicted in this regime.

Besides, isolas like Θ_c , formed through the merging of Θ_4^b and other Υ -like isolas [see Fig. 2(b)], appear, combining states like the one shown in Fig. 2(c).4 and Fig. 2(c).5. Indeed, the hybrid state shown in Fig 2(b).3 can be tracked by path-continuing the one depicted in Fig. 2(c).4.

V. DISSECTING THE TRANSITION: THE NECKING BIFURCATION

The questions that arise now is: how is this transition taking place? The destruction of one bifurcation structure and the reorganization of branches to form new ones is normally related with the merging and later splitting of solution branches occurring when modifying one or several control parameters of the system. Here, this re-connection takes place through a cascade of codim-2 *necking bifurcations* [35], hereafter N, like those shown in the close-up views of Fig. 2(d) [see $N_{1,2}^b$]. In each N, a pair of saddle-node bifurcations belonging to different structures, e.g., one to a homoclinic snaking and another one to an isola, collide leading to the re-connection of solution branches and the reorganization of the bifurcation structure [17]. An schematic representation of the unfolding of this bifurcation is illustrated in Fig. 3.

To better understand the implication of this bifurcation in the snaking transition, let us take a closer look to its appearance near the collapsed snaking regime. Figure 4(a) shows the modification of the first pair of saddle-node bifurcations $\text{SN}_{c,i}^{b;l,r}$ ($i = 1, 2$) in the (Δ, S) -parameter space. The bifurcations $\text{SN}_{c,2}^{b;l,r}$ (see red curve) undergo the necking bifurcation N_2^b which is shown in the close-up view. This bifurcation always appear together with a pair of cusp bifurcations that here we mark as $C_{c,2}^l$

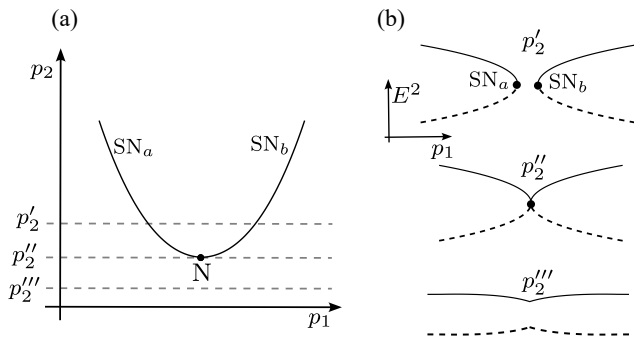


FIG. 3. **The necking bifurcation unfolding.** (a) Localization of the saddle-node bifurcations $SN_{a,b}$ in the parameter space (p_1, p_2) . In our case, we can consider $p_1 = S$ and $p_2 = \Delta$. The dashed lines indicate the fixed- p_2 slices depicted in (b) for $p = p'_2, p''_2$ and p'''_2 . The necking bifurcation N occurs at $p = p''_2$ when SN_a and SN_b collide.

and $C_{c,2}^r$.

Let us take a slice of Fig. 4(a) for $\Delta = 2.16$. The resulting bifurcation structure is shown in Fig. 4(b). Here, two main isolas appear: Θ_1^b and Υ' , both modifications of those already introduced in Fig. 2(b). A close-up view of this diagram (see right panel) shows how these isolas are disconnected, although very close to one another. There we can see two pairs of saddle-node bifurcations: $SN_{c,2}^{b;l}$ and $sn_{c,2}^{b;l}$ which are created at $C_{c,2}^l$, and $SN_{c,2}^{b;r}$ and $sn_{c,2}^{b;r}$ that emerge from $C_{c,2}^r$ [see Fig. 4(a)]. By increasing Δ further, $sn_{c,2}^{b;r}$ and $sn_{c,2}^{b;l}$ merge at $N_{c,2}^b$, leading to the re-connection of Θ_1^b and Υ' . This process yields the situation depicted in Fig. 4(c) for $\Delta = 2.3$, where two pre-collapsed snaking structures appear. The blue curve Σ will eventually lead to the collapsed snaking shown in Fig. 1(c) once the top part of the diagram connects with TI_2^+ . The violet curve Σ' corresponds to other type of mixed states, separated by $L/2$, which emanate from the small amplitude states with a hole in their center. Here, for simplicity we do not show such states and refer the interested reader to other works [7, 36].

This complex re-connection takes place in a cascade of necking bifurcation occurring in other parameter regimes. At low detuning, for example, a similar process leads to the destruction of the standard homoclinic snaking Γ_0^b and the consequent formation of isolas $\Theta_{1,2,3,4}^b$ [see Fig. 2(b)]. In this case, the bifurcation involved in such transition is N_1^b , and is marked in the close-up view of Fig. 2(d).

Although, we have just focused on the reorganization of the bottom part of the bifurcation diagrams shown in Fig. 2, similar bifurcation events occurs regarding the top part of such diagrams. This leads to an even more complex scenario, whose complete unfolding requires further study.

VI. DISCUSSIONS AND CONCLUSIONS

In one-dimensional extended system, the formation of LSs and their organization in the parameter space is dictated, in general, by the interaction of front waves between extended stable states which can be of different nature, and may involve two or even more different states.

When two stable states coexist, two main bifurcation organization appears: the standard and collapsed homoclinic snakings. These structures have been widely studied in different fields ranging from photonics to popula-

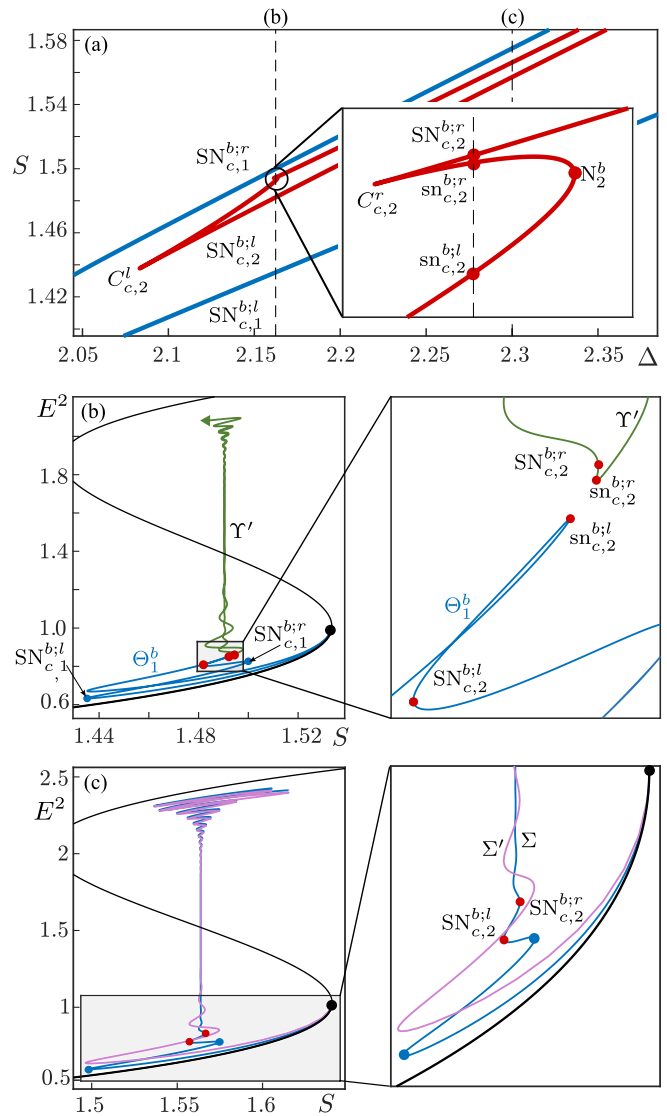


FIG. 4. **The necking bifurcation in the collapsed snaking formation.** Panel (a) shows the modification of $SN_{c,1}^b$ and $SN_{c,2}^b$, and the occurrence of the codim-2 bifurcations $C_{c,2}^l$, $C_{c,2}^r$ and the necking bifurcation $N_{c,2}^b$ in the (Δ, S) -parameter space. The vertical dashed lines correspond to the diagrams shown in panel (b) and (c) for $\Delta = 2.16$ and $\Delta = 2.3$, respectively. Panel (b) shows the situation just below the occurrence of $N_{c,2}^b$: the isolas Θ_1^b and Υ' are very close to one another. Panel (c) illustrates the situation above the collision of Θ_1^b and Υ' in $N_{c,2}^b$.

tion dynamics [8, 12–14, 16, 37]. Nowadays, one can say that both structures are quite well understood separately, and a strong mathematical framework supports this fact [5, 6, 8, 32, 38, 39].

In this article, we have analyzed the formation of LSs in Kerr passive cavities in tristable regimes where two uniform states coexist with an extended pattern. We have referred to this scenario as *uniform-pattern-uniform* tristable regime. For this analysis, we have considered the LLE which is traditionally used for understanding the spatiotemporal dynamics of light pulses in Kerr dispersive passive cavities [12, 20]. Here, such tristable regime emerges when the normalized dispersion coefficients are set to $d_2 = -1$ and $d_4 = 1$. This configuration was tackled, although only superficially, in previous works, where the existence of standard homoclinic snaking for dark and bright LSs was predicted [24]. Our present work, shows the existence of collapsed snaking and the complex transition between the former and the latter. Performing a systematic and detailed bifurcation analysis we show that this transition is mediated by a cascade of codim-2 *necking bifurcations* which are related to the emergence of new hybrid states.

This work, which focuses on a non-variational system, shows a similar bifurcation organization than those presented in variational (i.e., gradient-like) context [17] demonstrating that such transition is generic in 1D ex-

tended systems which are far from thermodynamics equilibrium.

Necking bifurcations have been also demonstrated in the context of fluid dynamics, particularly in two-dimensional Rayleigh–Bénard convection problems [35]. Besides, such bifurcations are responsible of the bifurcation scenario found in other pattern forming systems including plant population dynamics [14, 15].

Regarding the experimental demonstration of such states in a cavity optics context, the dispersion regime discussed here could be reached using advanced dispersion engineering techniques as those based, for example, on an intracavity pulse shaper [40]. This technique, initially proposed in the context of soliton lasers, opens astonishing possibilities and new avenues for LSs formation and control.

Regarding higher extended dimensions, it is unknown how this scenario could be generalized. This problem could be tackled in the case of radially symmetric states by continuing homotopically, in the system dimension, the LSs in 1D to 2D and 3D. Some studies of this kind have been performed regarding standard homoclinic related states in the Swift-Hohenberg equation [41] and spike-like solitons in passive cavities with parabolic potentials [42]. However, the transition shown here is completely unknown in those cases. We will address these question in future investigations.

-
- [1] Y. Pomeau, “Front motion, metastability and subcritical bifurcations in hydrodynamics,” *Physica D: Nonlinear Phenomena*, vol. 23, pp. 3–11, Dec. 1986.
- [2] P. Coullet, C. Elphick, and D. Repaux, “Nature of spatial chaos,” *Physical Review Letters*, vol. 58, pp. 431–434, Feb. 1987.
- [3] O. Thual and S. Fauve, “Localized structures generated by subcritical instabilities,” *Journal de Physique*, vol. 49, no. 11, pp. 1829–1833, 1988.
- [4] P. Coullet, “Localized patterns and fronts in nonequilibrium systems,” *International Journal of Bifurcation and Chaos*, vol. 12, pp. 2445–2457, Nov. 2002.
- [5] P. D. Woods and A. R. Champneys, “Heteroclinic tangles and homoclinic snaking in the unfolding of a degenerate reversible Hamiltonian–Hopf bifurcation,” *Physica D: Nonlinear Phenomena*, vol. 129, pp. 147–170, May 1999.
- [6] J. Knobloch and T. Wagenknecht, “Homoclinic snaking near a heteroclinic cycle in reversible systems,” *Physica D: Nonlinear Phenomena*, vol. 206, pp. 82–93, June 2005.
- [7] P. Parra-Rivas, E. Knobloch, D. Gomila, and L. Gelens, “Dark solitons in the Lugiato-Lefever equation with normal dispersion,” *Physical Review A*, vol. 93, p. 063839, June 2016.
- [8] D. Gomila, A. J. Scroggie, and W. J. Firth, “Bifurcation structure of dissipative solitons,” *Physica D: Nonlinear Phenomena*, vol. 227, pp. 70–77, Mar. 2007.
- [9] P. Parra-Rivas, D. Gomila, L. Gelens, and E. Knobloch, “Bifurcation structure of localized states in the Lugiato-Lefever equation with anomalous dispersion,” *Physical Review E*, vol. 97, p. 042204, Apr. 2018.
- [10] P. Parra-Rivas, L. Gelens, and F. Leo, “Localized structures in dispersive and doubly resonant optical parametric oscillators,” *Physical Review E*, vol. 100, p. 032219, Sept. 2019.
- [11] P. Parra-Rivas, C. Mas-Arabí, and F. Leo, “Parametric localized patterns and breathers in dispersive quadratic cavities,” *Physical Review A*, vol. 101, p. 063817, June 2020.
- [12] P. Parra-Rivas, E. Knobloch, L. Gelens, and D. Gomila, “Origin, bifurcation structure and stability of localized states in Kerr dispersive optical cavities,” *IMA Journal of Applied Mathematics*, vol. 86, pp. 856–895, Oct. 2021.
- [13] F. Al Saadi and A. Champneys, “Unified framework for localized patterns in reaction–diffusion systems; the Gray–Scott and Gierer–Meinhardt cases,” *Philosophical Transactions of the Royal Society A: Mathematical, Physical and Engineering Sciences*, vol. 379, p. 20200277, Dec. 2021. Publisher: Royal Society.
- [14] Y. R. Zelnik, P. Gandhi, E. Knobloch, and E. Meron, “Implications of tristability in pattern-forming ecosystems,” *Chaos: An Interdisciplinary Journal of Nonlinear Science*, vol. 28, p. 033609, Mar. 2018.
- [15] F. Al Saadi and P. Parra-Rivas, “Transitions between dissipative localized structures in the simplified Gilad–Meron model for dryland plant ecology,” *Chaos: An Interdisciplinary Journal of Nonlinear Science*, vol. 33, p. 033129, Mar. 2023.
- [16] H. Schmidt and D. Avitabile, “Bumps and oscillons in networks of spiking neurons,” *Chaos: An Interdisciplinary Journal of Nonlinear Science*, vol. 30, p. 033133, Mar. 2020.

- [17] P. Parra-Rivas, A. R. Champneys, F. A. Saadi, D. Gomila, and E. Knobloch, "Organization of Spatially Localized Structures near a Codimension-Three Cusp-Turing Bifurcation," *SIAM Journal on Applied Dynamical Systems*, pp. 2693–2731, Dec. 2023. Publisher: Society for Industrial and Applied Mathematics.
- [18] M. C. Cross and P. C. Hohenberg, "Pattern formation outside of equilibrium," *Reviews of Modern Physics*, vol. 65, pp. 851–1112, July 1993.
- [19] L. A. Lugiato and R. Lefever, "Spatial Dissipative Structures in Passive Optical Systems," *Physical Review Letters*, vol. 58, pp. 2209–2211, May 1987.
- [20] M. Haelterman, S. Trillo, and S. Wabnitz, "Dissipative modulation instability in a nonlinear dispersive ring cavity," *Optics Communications*, vol. 91, pp. 401–407, Aug. 1992.
- [21] M. Rowley, P.-H. Hanzard, A. Cutrona, H. Bao, S. T. Chu, B. E. Little, R. Morandotti, D. J. Moss, G.-L. Oppo, J. S. Toterogongora, M. Peccianti, and A. Pasquazi, "Self-emergence of robust solitons in a microcavity," *Nature*, vol. 608, pp. 303–309, Aug. 2022. Number: 7922 Publisher: Nature Publishing Group.
- [22] J. Lottes, G. Biondini, and S. Trillo, "Excitation of switching waves in normally dispersive Kerr cavities," *Optics Letters*, vol. 46, pp. 2481–2484, May 2021. Publisher: Optica Publishing Group.
- [23] Y. K. Chembo and C. R. Menyuk, "Spatiotemporal Lugiato-Lefever formalism for Kerr-comb generation in whispering-gallery-mode resonators," *Physical Review A*, vol. 87, p. 053852, May 2013.
- [24] M. Tlidi and L. Gelens, "High-order dispersion stabilizes dark dissipative solitons in all-fiber cavities," *Optics Letters*, vol. 35, pp. 306–308, Feb. 2010.
- [25] E. K. Akakpo, M. Haelterman, F. Leo, and P. Parra-Rivas, "Emergence of collapsed snaking related dark and bright Kerr dissipative solitons with quartic-quadratic dispersion," *Physical Review E*, vol. 108, p. 014203, July 2023. Publisher: American Physical Society.
- [26] P. Parra-Rivas, S. Hetzel, Y. V. Kartashov, P. F. d. Córdoba, J. A. Conejero, A. Aceves, and C. Milián, "Quartic Kerr cavity combs: bright and dark solitons," *Optics Letters*, vol. 47, pp. 2438–2441, May 2022. Publisher: Optica Publishing Group.
- [27] E. Doedel, H. B. Keller, and J. P. Kernevez, "Numerical analysis and control of bifurcation problems (ii): bifurcation in infinite dimensions," *International Journal of Bifurcation and Chaos*, vol. 01, pp. 745–772, Dec. 1991.
- [28] E. Doedel, H. B. Keller, and J. P. Kernevez, "Numerical analysis and control of bifurcation problems (i): bifurcation in finite dimensions," *International Journal of Bifurcation and Chaos*, vol. 01, pp. 493–520, Sept. 1991.
- [29] E. J. Doedel, A. R. Champneys, T. F. Fairgrieve, Y. A. Kuznetsov, B. Sandstede, and X. Wang, "AUTO-07p: Software for continuation and bifurcation problems in ordinary differential equations," *Department of Computer Science, Concordia University, Montreal*, 2007.
- [30] S. Wiggins, *Introduction to Applied Nonlinear Dynamical Systems and Chaos*. Texts in Applied Mathematics, New York: Springer-Verlag, 2 ed., 2003.
- [31] A. J. Scroggie, W. J. Firth, G. S. McDonald, M. Tlidi, R. Lefever, and L. A. Lugiato, "Pattern formation in a passive Kerr cavity," *Chaos, Solitons & Fractals*, vol. 4, pp. 1323–1354, Aug. 1994.
- [32] E. Makrides and B. Sandstede, "Existence and stability of spatially localized patterns," *Journal of Differential Equations*, vol. 266, pp. 1073–1120, Jan. 2019.
- [33] J. Burke and E. Knobloch, "Snakes and ladders: Localized states in the Swift–Hohenberg equation," *Physics Letters A*, vol. 360, pp. 681–688, Jan. 2007.
- [34] P. Parra-Rivas, D. Gomila, E. Knobloch, S. Coen, and L. Gelens, "Origin and stability of dark pulse Kerr combs in normal dispersion resonators," *Optics Letters*, vol. 41, pp. 2402–2405, June 2016.
- [35] J. Prat, I. Mercader, and E. Knobloch, "The 1:2 mode interaction in rayleigh–bénard convection with and without boussinesq symmetry," *International Journal of Bifurcation and Chaos*, vol. 12, pp. 281–308, Feb. 2002.
- [36] P. Parra-Rivas and C. Fernandez-Oto, "Formation of localized states in dryland vegetation: Bifurcation structure and stability," *Physical Review E*, vol. 101, p. 052214, May 2020.
- [37] J. M. T. Thompson, "Advances in Shell Buckling: Theory and Experiments," *International Journal of Bifurcation and Chaos*, Feb. 2015. Publisher: World Scientific Publishing Company.
- [38] G. Kozyreff and S. J. Chapman, "Asymptotics of Large Bound States of Localized Structures," *Physical Review Letters*, vol. 97, p. 044502, July 2006.
- [39] A. D. Dean, P. C. Matthews, S. M. Cox, and J. R. King, "Exponential asymptotics of homoclinic snaking," *Nonlinearity*, vol. 24, p. 3323, Oct. 2011.
- [40] A. F. J. Runge, D. D. Hudson, K. K. K. Tam, C. M. de Sterke, and A. Blanco-Redondo, "The pure-quartic soliton laser," *Nature Photonics*, vol. 14, pp. 492–497, Aug. 2020. Number: 8 Publisher: Nature Publishing Group.
- [41] S. McCalla and B. Sandstede, "Snaking of radial solutions of the multi-dimensional Swift–Hohenberg equation: A numerical study," *Physica D: Nonlinear Phenomena*, vol. 239, pp. 1581–1592, Aug. 2010.
- [42] Y. Sun, P. Parra-Rivas, M. Zitelli, F. Mangini, M. Ferraro, and S. Wabnitz, "2 - An introduction to guided-wave nonlinear ultrafast photonics," in *Advances in Nonlinear Photonics* (G. C. Righini and L. Sirleto, eds.), Woodhead Publishing Series in Electronic and Optical Materials, pp. 27–55, Woodhead Publishing, Jan. 2023.